REPORT DOCUMENTATION PAGE

Form Approved OMB NO. 0704-0188

1. REPORT DATE (DD-MM-YYYY)	2. REPORT TYPE	3. DATES COVERED (From - To)
07-01-2011	Final Report	1-Sep-2006 - 31-Aug-2010

4. TITLE AND SUBTITLE
Voltage-Tunable High-Q Acoustic Resonators for RF Applications

5a. CONTRACT NUMBER
W911NF-06-1-0431

5b. GRANT NUMBER

5c. PROGRAM ELEMENT NUMBER
611102

6. AUTHORS
Robert York

5d. PROJECT NUMBER

5e. TASK NUMBER

5f. WORK UNIT NUMBER

7. PERFORMING ORGANIZATION NAMES AND ADDRESSES
University of California - Santa Barbara
Office of Research
The Regents of the University of California
Santa Barbara, CA 93106 -2050

8. PERFORMING ORGANIZATION REPORT NUMBER

9. SPONSORING/MONITORING AGENCY NAME(S) AND ADDRESS(ES)
U.S. Army Research Office
P.O. Box 12211
Research Triangle Park, NC 27709-2211

10. SPONSOR/MONITOR'S ACRONYM(S)
ARO

11. SPONSOR/MONITOR'S REPORT NUMBER(S)
51085-EL.1

12. DISTRIBUTION AVAILIBILITY STATEMENT
Approved for Public Release; Distribution Unlimited

13. SUPPLEMENTARY NOTES
The views, opinions and/or findings contained in this report are those of the author(s) and should not contrued as an official Department of the Army position, policy or decision, unless so designated by other documentation.

14. ABSTRACT
The electrostrictive property of thin-film strontium titanate (STO) and barium strontium titanate (BST) is manifest as a voltage-induced piezoelectricity. During the four years of this award the PI proposed and successfully demonstrated a new type of voltage-activated bulk-acoustic-wave (VBAW) resonator to exploit this effect. These new type of devices could form the building block for a new class of high-performance reconfigurable RF filters. The final report outlines the basic concept and progress achieved during the program towards the goal of

15. SUBJECT TERMS
Acoustic Resonators, BAW, RF filters

16. SECURITY CLASSIFICATION OF:			17. LIMITATION OF ABSTRACT	15. NUMBER OF PAGES	19a. NAME OF RESPONSIBLE PERSON
a. REPORT	b. ABSTRACT	c. THIS PAGE			Robert York
UU	UU	UU	UU		19b. TELEPHONE NUMBER 805-893-7113

Report Title

ABSTRACT

The electrostrictive property of thin-film strontium titanate (STO) and barium strontium titanate (BST) is manifest as a voltage-induced piezoelectricity. During the four years of this award the PI proposed and successfully demonstrated a new type of voltage-activated bulk-acoustic-wave (VBAW) resonator to exploit this effect. These new type of devices could form the building block for a new class of high-performance reconfigurable RF filters. The final report outlines the basic concept and progress achieved during the program towards the goal of implementing useful reconfigurable filter structures.

List of papers submitted or published that acknowledge ARO support during this reporting period. List the papers, including journal references, in the following categories:

(a) Papers published in peer-reviewed journals (N/A for none)

"Improvement of Barium Strontium Titanate Solidly Mounted Resonator Quality Factor By Reduction in Electrode Surface Roughness",
Journal of Applied Physics,
Accepted August 2010
Authors: George N. Saddik, Junwoo Son, Susanne Stemmer and Robert A. York

Number of Papers published in peer-reviewed journals: 1.00

(b) Papers published in non-peer-reviewed journals or in conference proceedings (N/A for none)

Number of Papers published in non peer-reviewed journals: 0.00

(c) Presentations

Number of Presentations:

Non Peer-Reviewed Conference Proceeding publications (other than abstracts):

Number of Non Peer-Reviewed Conference Proceeding publications (other than abstracts):

Peer-Reviewed Conference Proceeding publications (other than abstracts):

Number of Peer-Reviewed Conference Proceeding publications (other than abstracts):

(d) Manuscripts

Number of Manuscripts:

Patents Submitted

Patents Awarded

Awards

Graduate Students

NAME	PERCENT_SUPPORTED
George N. Saddik	0.90
FTE Equivalent:	**0.90**
Total Number:	**1**

Names of Post Doctorates

NAME	PERCENT_SUPPORTED
FTE Equivalent:	
Total Number:	

Names of Faculty Supported

NAME	PERCENT_SUPPORTED	National Academy Member
Robert York	0.10	No
FTE Equivalent:	**0.10**	
Total Number:	**1**	

Names of Under Graduate students supported

NAME	PERCENT_SUPPORTED
FTE Equivalent:	
Total Number:	

Student Metrics

This section only applies to graduating undergraduates supported by this agreement in this reporting period

The number of undergraduates funded by this agreement who graduated during this period:	0.00
The number of undergraduates funded by this agreement who graduated during this period with a degree in science, mathematics, engineering, or technology fields:.....	0.00
The number of undergraduates funded by your agreement who graduated during this period and will continue to pursue a graduate or Ph.D. degree in science, mathematics, engineering, or technology fields:.....	0.00
Number of graduating undergraduates who achieved a 3.5 GPA to 4.0 (4.0 max scale):	0.00
Number of graduating undergraduates funded by a DoD funded Center of Excellence grant for Education, Research and Engineering:	0.00
The number of undergraduates funded by your agreement who graduated during this period and intend to work for the Department of Defense	0.00
The number of undergraduates funded by your agreement who graduated during this period and will receive scholarships or fellowships for further studies in science, mathematics, engineering or technology fields:	0.00

Names of Personnel receiving masters degrees

NAME
Total Number:

Names of personnel receiving PHDs

NAME

Total Number:

Names of other research staff

NAME PERCENT_SUPPORTED

FTE Equivalent:

Total Number:

Sub Contractors (DD882)

Inventions (DD882)

Scientific Progress

See Attachment

Technology Transfer

Final Report, August 2010
ARO Proposal 51085-EL, Agreement W911NF0610431
Voltage-Tunable High-Q Acoustic Resonators for RF Applications
PI: Bob York, UCSB rayork@ece.ucsb.edu
Start date: 9/1/2006 End date: 8/31/2010

Foreword

The electrostrictive property of thin-film strontium titanate (STO) and barium strontium titanate (BST) is manifest as a voltage-induced piezoelectricity [1]-[4]. During the four years of this award the PI proposed and successfully demonstrated a new type of voltage-activated bulk-acoustic-wave (VBAW) resonator to exploit this effect [5]-[7], and similar work has now been reported by other researchers [8]-[13]. These new type of devices could form the building block for a new class of high-performance reconfigurable RF filters. This report will outline the basic concept and progress achieved during the program towards the goal of implementing useful reconfigurable filter structures.

Key Terms/Abbreviations/Acronyms:

BAW: Bulk Acoustic Wave
VBAW: Voltage-Activate Bulk Acoustic Wave (technology proposed herein)
ABR: Acoustic Bragg Reflector. A high reflectivity "mirror" for acoustic waves formed using alternating layers of high and low impedance materials.
SMR: Solidly-Mounted Resonator: a BAW device fabricated on an ABR.
FBAR: Film Bulk Acoustic Device: A BAW device suspended on a thin membrane.
BST: Barium Strontium Titanate
STO: Strontium Titanate

Table of Contents

List of Illustrations and Tables

Statement of the Problem Studied

The design and fabrication of a new class of voltage-activated BAW devices using thin-film STO and BST materials was studied. At the start of the program there was experimental evidence of the underlying electrostrictive property, but no devices had yet been demonstrated to isolate the mechanical resonance from the damping effects of the substrate. The essence of the program was therefore to solve this problem and also identify and minimize other sources of loss, and then to explore ways to exploit such devices in a functional integrated filter circuit.

A Brief Introduction to Piezoelectric BAW Resonators

Piezoelectric resonators have been used for decades to realize high-Q filters and low-loss, narrow-band frequency-selective networks [14,15]. There are two main types of piezoelectric devices: surface acoustic wave (SAW) devices, and bulk-acoustic-wave (BAW) devices [16]. We focused on BAW devices as this is the configuration that most easily exploits the voltage-controlled piezoelectricity of strontium titanate (STO) and Barium Strontium Titanate (BST).

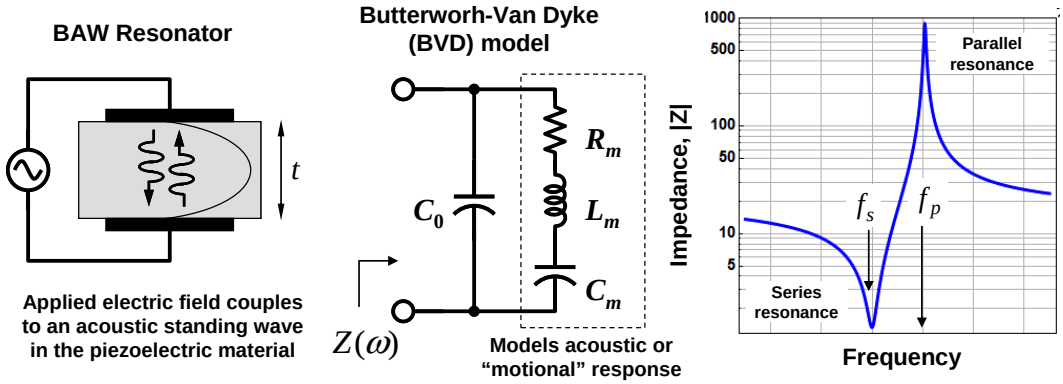

Figure 1 – (a) Basic BAW resonator structure. (b) Narrowband electrical model for the device, valid in the vicinity of the resonance. (c) Impedance behavior at or near the fundamental resonances.

Figure 1a illustrates the basic structure of a BAW resonator. BAWs are designed so that the thickness of the piezoelectric material is $\lambda/2$ where λ is the *acoustic* wavelength ($\lambda = v_s / f$, and v_s is the velocity of sound in the material). When a time-varying electric field is applied it couples to an acoustic standing wave by virtue of the piezoelectric property of the material. When the frequency of the electrical signal coincides with an acoustic resonance mode, a strong coupling of energy can take place and a sharp resonance is observed in the electrical circuit, modeled by the Butterworth-Van Dyke circuit in Figure 1b [17]. Since the device is a metal-dielectric-metal sandwich there is always some intrinsic capacitance C_0 which leads to a secondary parallel or "anti" resonance above the series resonance. Thus the input impedance of such resonators has the behavior shown in Figure 1c, displaying a small impedance at the series resonance f_s and a large impedance at the parallel resonance f_p. All BAW filters are design to exploit one or both of these resonances.

There are two key empirical figures of merit for BAW devices: 1) the effective electromechanical coupling coefficient, $k^2_{t,eff}$, which describes the strength of the coupling between the applied electric field and the acoustic mode, and 2) the quality-factor or Q-factor of the resonator, which is the ratio of stored energy to average power dissipated. Both parameters can be determined experimentally by fitting data to a BVD model. Alternatively, $k^2_{t,eff}$ can be related to the measured resonance frequencies as [17]

$$k^2_{t,eff} = \frac{\pi}{2}\frac{f_s}{f_p}\cot\left(\frac{\pi}{2}\frac{f_s}{f_p}\right) \approx \frac{\pi^2}{4}\frac{f_s}{f_p}\left(\frac{f_p - f_s}{f_p}\right) \qquad (1)$$

and the Q-factor at each resonance can be related to the slope of the measured impedance phase as

$$Q = \frac{\omega}{2}\frac{\partial\theta}{\partial\omega}\bigg|_{\omega_s,\omega_p} \qquad \text{where} \quad \theta = \arg\{Z(\omega)\} \tag{2}$$

It can be shown [17] that the BVD model parameters are then given by

$$C_m = \frac{8k_{t,eff}^2}{\pi^2}C_0 \qquad L_m = \frac{1}{C_m(2\pi f_s)^2} \qquad R_m = \frac{\alpha_{eff}}{\pi f_s C_m} \tag{3}$$

where f_s is the resonant frequency of the series branch (set by the material thickness), and α_{eff} is an effective attenuation factor that can be related to the device Q-factor (more on that later). Many commercial BAW devices now use sputtered aluminum nitride films with thin aluminum electrodes, featuring a $k_{t,eff}^2$ of 6.5% and Q-factors of >2000 [15].

For the resonator to function properly the top and bottom surfaces must be highly reflective to the acoustic waves resulting in a "free" resonator with the highest possible Q-factor. However, every practical resonator has a support structure which tends to damp the mechanical resonance, lowering the Q-factors. The two most common ways of isolating the device from its support structure are shown in Figure 2. The first (Figure 2a) is commonly called a *thin film bulk acoustic resonator* (FBAR) topology, where a cavity is formed underneath the resonator. The second (Figure 2b) is called a *solidly-mounted resonator* (SMR) structure, employing a distributed Bragg reflector or acoustic "mirror" under the device. Both approaches yield similar results and are commonly used in mobile wireless handset front-ends to realize low-loss and high-selectivity duplexers [18].

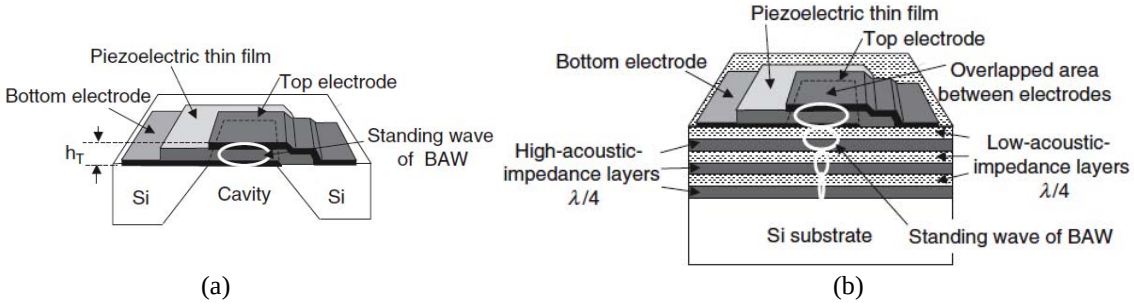

Figure 2 – Two common techniques [18] to isolate the acoustic resonator from the mechanical damping effects of the substrate: (a) Film bulk Acoustic Resonator (FBAR); (b) Solidly-Mounted Resonator (SMR).

The Voltage-Activated BAW Concept

Existing BAW devices are fixed-frequency devices. For multi-band or multi-mode communications, frequency-agile or reconfigurable components are highly desirable, but until recently there has been no known method of creating high-Q voltage-controlled components. All known tuning technologies (varactors, MEMS, tunable dielectrics, and ferrites) have rather low Q-factors at RF frequencies, and always involve a tradeoff between the parameter being varied (e.g. device capacitance) and the Q-factor.

Serendipitously, two of the thin-film materials used in the exploration of tunable dielectric devices were found to exhibit an apparent *field-induced piezoelectricity*, observed as resonances in the frequency response under DC bias. This was first reported in thin-film strontium titanate (STO) devices [3] and then later in barium strontium titanate (BST) devices [4] and subsequently attributed to an *electrostrictive* property of the materials, which probably should have been anticipated much earlier since it had been demonstrated in similar bulk ceramic materials long ago [1,2]. The term "electrostrictive" distinguishes the observed effects from an ordinary piezoelectric material which does not require DC bias and also exhibits the inverse effect (mechanical deformation leading to an electrical polarization).

More recently, we and a number of other researchers have begun to develop BAW devices that exploit this electrostrictive property [5]-[13]. We refer to this herein as a *voltage-activated BAW technology*, or

VBAW. VBAW devices differ from conventional BAW devices in that the acoustic resonance can be switched "on" or "off" by the application or removal of a DC electric field. Under bias, thin-film STO and BST becomes piezoelectrically active, and RF coupling to a thickness-mode acoustic resonance is observed; subsequent removal of the DC bias renders the device piezoelectrically inactive, and no resonance is observed (the device is simply an ordinary capacitor at zero bias).

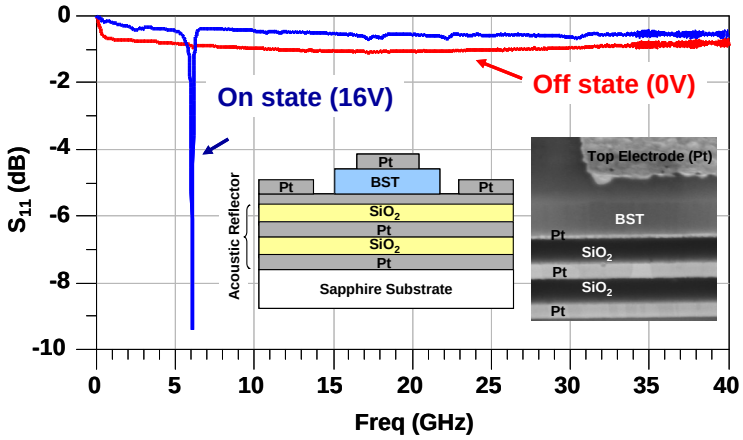

Figure 3 – Example data for a BST-based voltage-activated acoustic resonator fabricated at UCSB on a Pt-SiO_2 Bragg reflector, illustrating the ability to control the resonance with a DC field. Note that this particular data was selected to visually emphasize the on-off switching characteristic; a practical resonator for high-Q filters would not be matched to 50Ω.

Figure 3 illustrates recent data on a BST-based voltage-activated BAW device developed during this program. This figure illustrates that the acoustic resonance only appears under the application of DC bias to the device. By incorporating a number of such devices in a filter circuit, high-Q reconfigurable filters can be constructed. The key advantage of VBAWs over conventional filters is the integration of this switching/tuning function, as well as an inherent size advantage (BST-based BAWs occupy an order of magnitude smaller area than conventional AlN devices). Thus this technology appears to have significant promise for a new generation of compact, high-Q reconfigurable or frequency-agile filters.

Summary of Important Results

Significant progress was been made in developing this technology, summarized as follows:

- Developed circuit models and a library of key material parameters for device modeling, data extraction, and circuit design.
- Successful development and implementation of a robust Pt/SiO_2 mirror stack to withstand high-temperature BST/STO growth (up to 800C) without hillock formation or delamination.
- Demonstrated both BST- and STO-based resonators on 4-layer mirror structures with resonator Q-factors up to 130.
- Preliminary investigation of important loss contributions (interfacial roughness, viscous damping in electrodes) and demonstration of some promising solutions
- Quantified the influence of BST loss tangent and parasitic series losses on BAW device performance to show that these are not serious limitations fro the technology.
- Improved thickness control of mirror layers and BST/STO.
- Demonstrated devices with alternative mirror and electrode materials and identified promising options for future work
- Most importantly, we have demonstrated the first (albeit rudimentary) filter circuits and shunt-series resonators using this technology.

This work validated the basic concept of voltage-activated BAW devices but also identified key areas for improvement. The following reviews these results in more detail.

Physical Modeling of BAW Structures

Although the BVD model predicts the general behavior of acoustic devices, more sophisticated models are required to understand the role of each layer in complex multilayered devices like FBARs and SMRs and also to predict the broadband performance. Our approach follows [17] and uses an equivalent transmission-line model for each layer. Every material layer (including electrodes, dielectrics, substrates, etc) is specified by a mass density ρ_m acoustic velocity v_p, and mechanical viscosity η, from which an equivalent characteristic impedance Z_0 and complex propagation constant γ can be computed as follows [17]

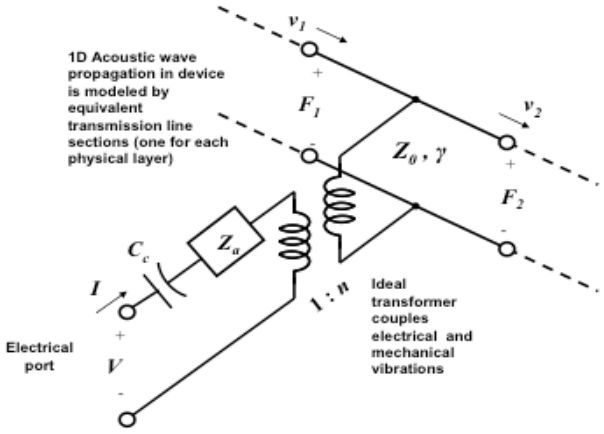

Figure 4 – KLM model for piezoelectric devices [9].

$$Z_0 = A\rho_m v_p \qquad \beta = \frac{\omega}{v_p} \qquad \alpha = \frac{\eta\omega}{2\rho_m v_p^2} \qquad \gamma = \alpha\beta + j\beta \tag{4}$$

where A is the active device area (electrode area). In addition, the active piezoelectric layer is characterized by a piezoelectric strain constant d_m[C/N] which relates the applied electric field to the resulting mechanical strain (deformation). The KLM model [19] of Figure 4 is conceptually and numerically attractive for modeling the electric-acoustic interaction because it can easily accommodate any number of physical layers, reducing the analysis to an equivalent electrical problem that can be solved on most RF circuit simulators (e.g. Agilent' Advanced Design System or AWR's Microwave Office). The equivalent circuit parameters in the KLM model are given by

$$Cc = \frac{\varepsilon A}{t} \qquad n = \frac{j\omega}{2h}\frac{Z_0}{\sinh(\gamma l/2)} \qquad Z_a = \frac{h^2}{\omega^2}\frac{\sinh\gamma l}{Z_0} \qquad \text{where} \quad h = \frac{c_m d_m}{\varepsilon - c_m d_m^2} \tag{5}$$

and c_m is the stiffness constant (Young's modulus) related to the mass density and acoustic velocity as $c_m = \rho_m v_p^2$.

Since the piezoelectric strain constant often appears in combination with other parameters, piezoelectric materials are often characterized by a dimensionless *piezoelectric coupling constant* K^2, or the *electromechanical coupling constant* k_t^2, related by

$$K^2 = h d_m \qquad k_t^2 \equiv \frac{K^2}{K^2+1} \qquad \frac{c_m d_m^2}{\varepsilon} \tag{6}$$

In can be shown that the BVD model described earlier is a narrowband equivalent circuit that can be derived from the KLM model by linearizing the expressions near the resonant frequency. Since the BVD model describes the aggregate response of the device (including acoustic contributions from all layers), the parameters $k_{t,eff}^2$ and α_{eff} in (3) are *effective* model parameters and may differ significantly from the coupling coefficient and attenuation factor of the piezoelectric layer alone.

By characterizing the device at a number of bias points and fitting the data to a KLM or BVD model, the coupling coefficient can be extracted for the film as a function of the applied DC field. This is shown

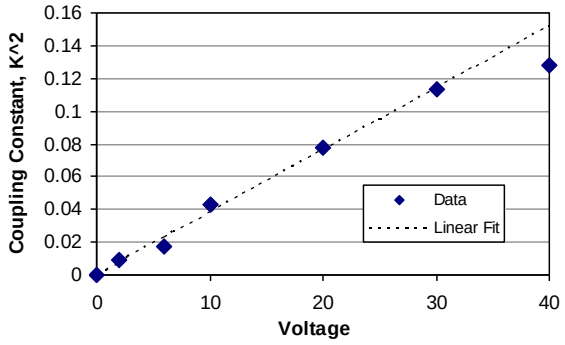

Figure 5 – Extracted piezoelectric coupling constant versus voltage for a BST thin film.

in Figure 5 for a thick BST film where the electrode thicknesses represented a relatively small fraction of the device thickness. In general we always observe a remarkably linear bias dependence of $k^2_{t,eff}$. This and other acoustic parameters of BST are contrasted with commonly-used piezoelectric materials in Table 1. Note that the electromechanical coupling constant is comparable to some of the best known piezoelectric materials including AlN, the workhorse of modern commercial BAW technology. The exciting difference here, of course, is that the coupling constant can be varied with an applied field, and is negligible with no applied field. There are still some parameters (acoustic velocity and viscosity) that are not known precisely and continue to be refined with every new experiment.

Table 1 – Comparison of extracted BST parameters with other common piezoelectric materials

	Mass Density ρ_m [g/cm^3]	Acoustic Velocity v_p [m/s]	Coupling Constant k_t^2	Dielectric Constant ε_r	Viscosity η
ZnO	**5.68**	**6,340**	**0.078**	**9.16/12.6**	**5×10^{-3}**
AlN	**3.26**	**11,050**	**0.065**	**8.5**	**20×10^{-3}**
$LiNbO_3$	**4.64**	**7,400**	**0.25**	**44**	
PZT-4	**7.5**	**4,600**	**0.20**	**350**	
BST	**5.3-5.9**	**6,000-7,000**	**0 @ 0V bias 0.1 @ 1 MV/cm**	**300 @ 0 V**	**??**

Material and Processing Challenges

Most of the early research effort centered on the development of a suitable acoustic Bragg reflector (ABR) technology to isolate the resonator from the damping effects of the substrate. Initial attempts focused on the use of alternating layers of Pt and SiO_2. The high deposition temperatures required for sputter-deposition of BST (>600°C) coupled with the inherent CTE mismatches in ABR systems can lead to delamination and/or "hillocking"; this was overcome by carefully optimizing the deposition processes and post-deposition heat treatments for both materials. It is also important to carefully calibrate the growth rates so that the mirror thicknesses (nominally a quarter-wavelength) can be controlled accurately.

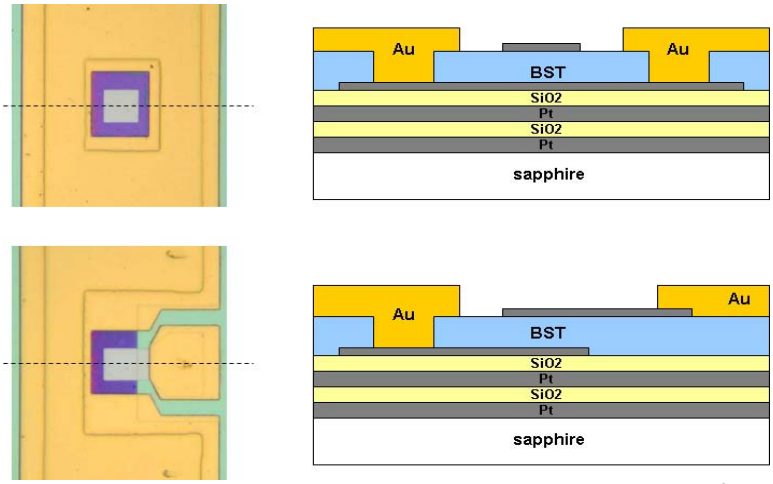

Figure 6 – Microscope photograph of two test structures with active area $(30\mu m)^2$, and schematic cross sections along dotted lines. The device in the top photo can be directly probed at the expense of probe-related damping. The bottom device gives an undamped top surface at the expense of larger series resistance.

For routine device and material characterization we typically use the simple test structures shown in Figure 6. These structures are attractive because they require minimal processing but have significant known limitations in terms of resistive and capacitive parasitics. In addition, rather rude lithographic

design rules were used for these devices in most of our experiments to date. Nevertheless many of these parasitic effects can be characterized readily and de-embedded from the data to yield useful information on the intrinsic BAW device, which is affected by materials and processing as follows:

- Surface roughness associated with the top and bottom surfaces of the active (BST layer): this leads to acoustic scattering losses
- Elastic-viscous damping loss in each layer relating to the choice of materials. This is believed to be especially problematic in the Pt electrodes.
- The use of unpatterned mirrors, which does not adequately confine the acoustic energy laterally. This is exacerbated by scattering losses associated with interfacial roughness.
- Excitation of undesired shear waves, which propagate in the device at a different acoustic velocity. This ultimately requires adjustments to ABR layer thicknesses as well an improved crystal orientation in the BST films.

The impact of interfacial roughness can be characterized by an attenuation factor given by [20]-[22]

$$\alpha_{rough}[\mathrm{dB}/\mu\mathrm{s}] = -4.34\frac{10^{-6}}{2d}V_s 4\pi\left(q^2 r_1^2 \quad q^2 r_2^2\right) \tag{7}$$

where r_1 and r_2 are the mean surface roughness of the top and bottom layers of the piezoelectric layer (the BST layer in this case). After data analysis we determined that the SiO_2 layers could be a significant contributor to the surface roughness of top mirror surface, and subsequently implemented improvements in this regard by moving to a slightly different CVD deposition method and a post-deposition "densification" step.

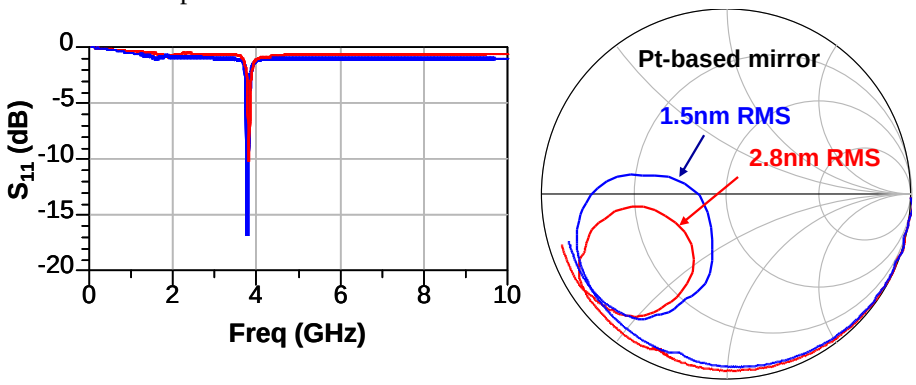

Figure 7 – Data comparing two devices with different levels of RMS surface roughness measured on the bottom electrode prior to BST deposition. The devices are otherwise identical in terms of design and resonant frequency. Smoother films clearly show an improvement in quality factor.

Evidence for the effects of surface roughness are shown in Figure 7, comparing two similar devices that differ ostensibly in only the surface roughness of the bottom electrode. Note that the quality-factor of acoustic resonators can be calculated numerically as in (2), but graphically is proportional to the size of the impedance loop on the Smith chart (larger loop = larger Q).

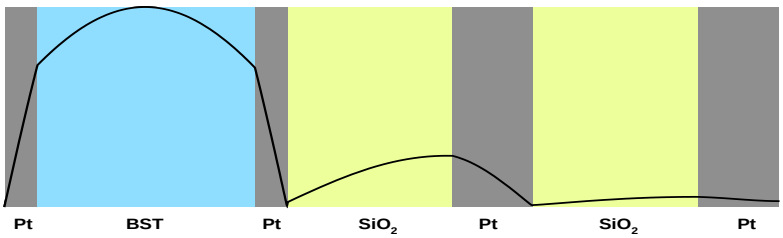

Figure 8 – Calculation (black line) of the stress distribution in each material layer at resonance, with the vertical scale representing the magnitude of the stress. Most of the viscous damping losses are associated with the top layers of the mirror, the piezoelectric layer, and especially the top/bottom electrodes.

The amount of elastic-viscous damping in each layer is related to the choice of materials as well as the distribution of acoustic energy in each layer. This damping is characterized by a "viscosity" constant η which contributes to the attenuation constant in each layer as specified in (4). An analysis of the magnitude of mechanical stress in each layer for our Pt-SiO_2 structure is shown in Figure 8. Since Pt is a high-impedance material, the use of Pt in the electrodes on either side of the BST results in significant energy in those layers and hence significant elastic-viscous damping losses.

In general the viscosity parameter is not well known or published for most materials, and it is nearly impossible to determine the relative contribution of each layer from measured data on a composite device. However, there is enough published data to suspect that platinum has rather poor performance in this respect relative to other materials, and conversely that SiO_2 (which is commonly used in commercial BAW devices) has relatively low damping losses. So the most effective way to reduce these losses would be to replace the platinum with an alternative high-impedance material in the mirrors, and with an alternative low-impedance conductor in the top/bottom electrodes. Consequently we explored tungsten and molybdenum as alternatives for the high-impedance mirror layer [6]. Figure 9 shows the basic structure using 580nm BST films on 2-period (4-layer) ABRs and Figure 10 summarizes the recent data. Raw Q-factors of 100 or better were achieved with both tungsten and "smooth" platinum-based mirrors. Note that this is not an apples-to-apples comparison in that the RMS roughness for each mirror was not uniform from sample to sample, and the acoustic impedance for each material also varies so the reflectivity of each mirror is different. However, the data is encouraging in the sense that our first attempts with tungsten and molybdenum mirrors yielded results that were comparable to the best Pt-based mirrors, for which considerably more effort in optimization had been invested. The data also shows that the piezoelectric coupling constants are roughly identical in each case, indicating that the BST film quality is relatively independent of the choice of mirror materials. The relatively low effective coupling constants were due to extrinsic parasitics.

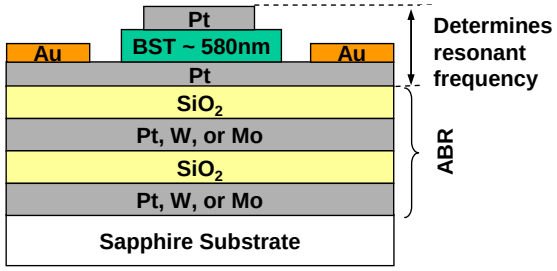

Figure 9 – Device cross section.

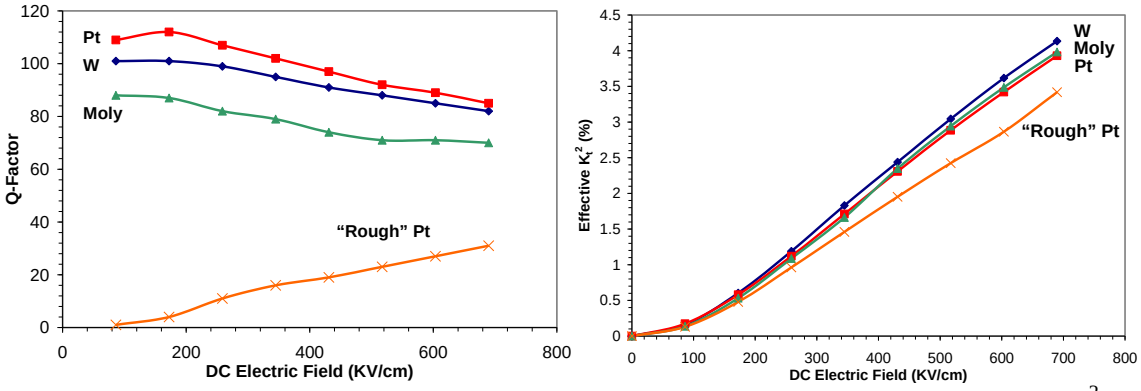

Figure 10 – Comparison of field-dependent Q-factors and piezoelectric coupling coefficients (k_t^2) for devices using 2-period (4-layer) mirrors with various high-impedance materials. This is raw data (no attempt was made at deembedding parasitic losses) which partially explains the low $k_{t,eff}^2$.

Device Parasitics and Fundamental Limits

Resistance due to the metal contacts and dielectric loss in the BST are the primary external parasitics. In the absence of these the Q-factor of the BAW resonator would be limited only to acoustic losses expressed through an effective attenuation factor in the BVD model as in (3), and this in turn can be related to the intrinsic acoustic Q-factor of the device as

$$Q_a = \frac{1}{2\alpha_{eff}} \qquad (8)$$

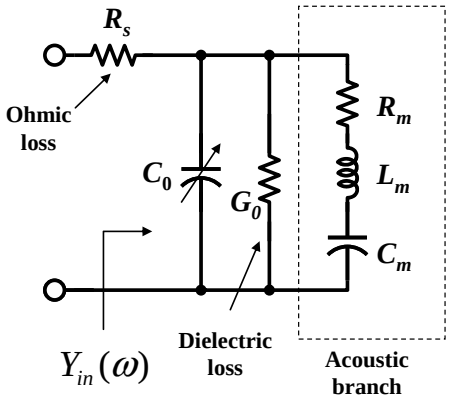

Figure 11 – Modified BVD model with series resistance and dielectric losses.

The parasitic losses associated with series resistance and loss tangents will reduce the Q further, so it is desirable to quantify this impact. Figure 11 illustrates a modified BVD model that adds these parasitics. Although the effects of a series resistance on the series Q-factor have been treated elsewhere, the effects of dielectric loss are not widely discussed so we have analytically derived an expression to quantify the impact of loss tangent. By definition the parallel conductance associated with dielectric loss is given by $G_0 = \omega C_0 \tan\delta = \omega C_0 / Q_d$, where $Q_d = 1/\tan\delta$ is the quality-factor associated with the dielectric loss, which we refer to as the "film-Q". For STO and BST, the film-Q increases under bias to some extent, typically beginning around 100 at 0V and increasing to >200 under bias. Solving for the total input admittance $Y_{in}(\omega)$ in the modified BVD model and using (2) we find that the series and parallel Q-factors are given by

$$Q_s \approx \frac{\omega_s L_m}{R_s + R_m} = \frac{1}{2\alpha_{eff} + \omega_s R_s C_0 \frac{8k_t^2}{\pi^2}} \qquad Q_p \quad \frac{1}{2\alpha_{eff} + \frac{8k_t^2}{\pi^2}\tan\delta} \qquad (9)$$

Interestingly the loss tangent and electrode losses are both multiplied by $k_{t,eff}^2$, explaining why it is possible to achieve BAW Q-factors that exceed the Q-factors normally associated with capacitors made from these materials. In the limit of very small acoustic losses, the maximum parallel Q-factor is

$$Q_{p,\max} \approx \frac{1}{\frac{8k_t^2}{\pi^2}\tan\delta} = \frac{\pi^2}{8k_t^2} Q_d \qquad (10)$$

Taking a conservative film-Q of $Q_d = 100$ for BST and a $k_{t,eff}^2$ of 5%, (10) gives loss-tangent-limited Q of >2000. Clearly the loss tangent of the films is not likely to be a significant limitation, and the observed loss in voltage-activated BAWs are largely due to acoustic losses and other parasitics. Interestingly, our analysis shows that when parasitic losses are included in the analysis, a large $k_{t,eff}^2$ tends to degrade the maximum achievable Q to a small extent. This partly explains the slow decrease in Q-factors observed at higher bias levels in Figure 10. So there is likely an optimum bias point for a given filter design using this technology.

Device and Circuit Results

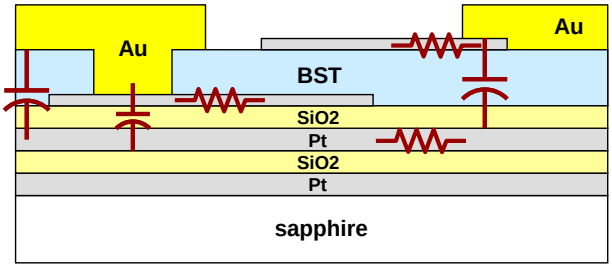

Figure 12 – Illustration of resistive and capacitive device parasitics in the simple test structures.

The data presented thus far has all been raw as-measured data on the test structures in Figure 6. These devices are useful for short-loop experiments, but as the technology has improved the shortcomings have become increasingly apparent. The key electrical parasitics are displayed in Figure 12. The thin top and bottom electrodes add series resistance which limits the series-Q as described in the previous section. It is not possible to eliminate this parasitic entirely, but it can be drastically reduced by moving to tighter lithographic design rules and better device layout. Using

an unpatterned "blanket" mirror also results in undesirable parasitic coupling between the contacts through the buried Pt-mirror layer.

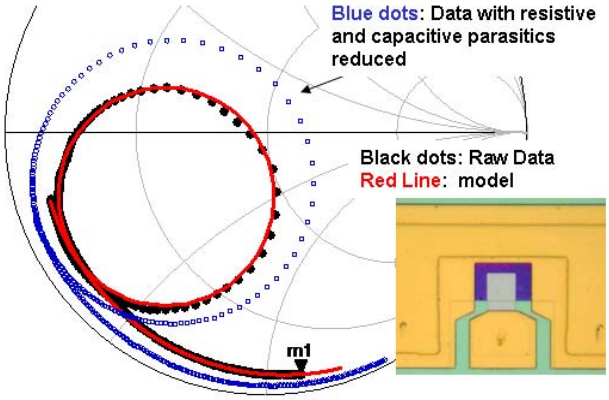

Figure 13 – Illustration of the impact of device parasitics on a simple $(30\mu\text{m})^2$ test structure used in the research efforts to date. Black dots are raw measured data; red line is the model with parasitics; blue is with parasitics reduced to a level that can be achieved with better device layout and finer lithographic design rules.

As mentioned earlier these resistive and capacitive parasitics can be easily characterized with suitable test structures and fitting the data to electrical circuit models, and this allows us to effectively de-embed the device from these parasitics.

Figure 13 illustrates the expected improvement that would be obtained just from improving the device layout only. Clearly moving towards a more sophisticated process and device layout must be a key feature of a future work effort.

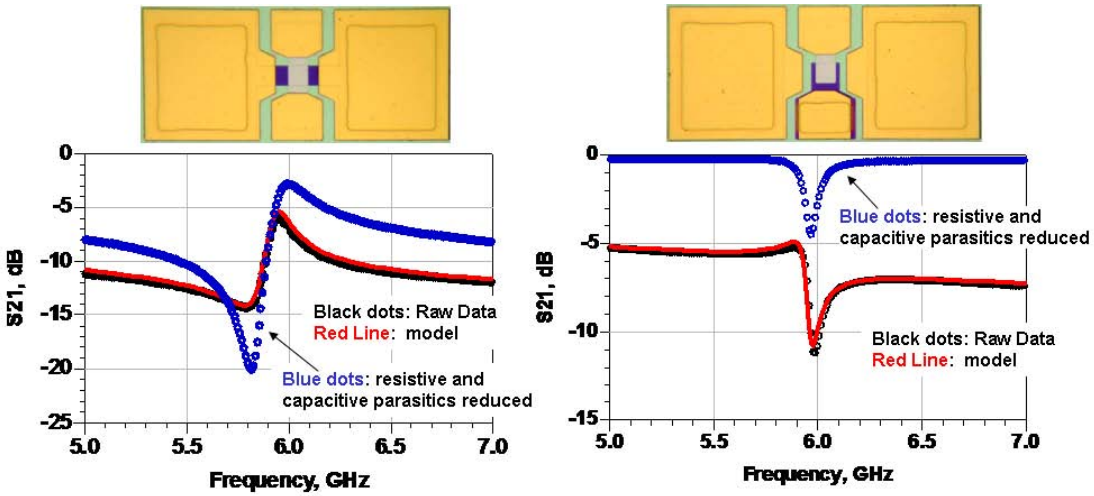

Figure 14 – Impact of device parasitics on the measured performace of a device(a) Two-port shunt resonator, and (b) two-port series resonator.

Figure 14 show photos and data for resonators in a basic two-port shunt and series configuration. These devices used 300nm BST films with 50nm Pt electrodes on the 4-layer Pt-SiO_2 mirror discussed earlier. The data shows excellent agreement with models incorporating the parasitic resistances and capacitances, and the figure also shows the expected improvement with those devices reduced in an improved layout. Figure 15 similarly illustrates a simple tee-filter which combines the series and shunt element of Figure 14. Ordinarily, commercial BAW filters use a mass-loading layer on the shunt elements to shift the resonant frequency, but here the separation of resonant frequencies in the series and shunt elements was obtained by a thickness variation in the BST film. The reason that the response dips in the passband is because the thickness variation was too large, and consequently the series and shunt device resonance were too far apart.

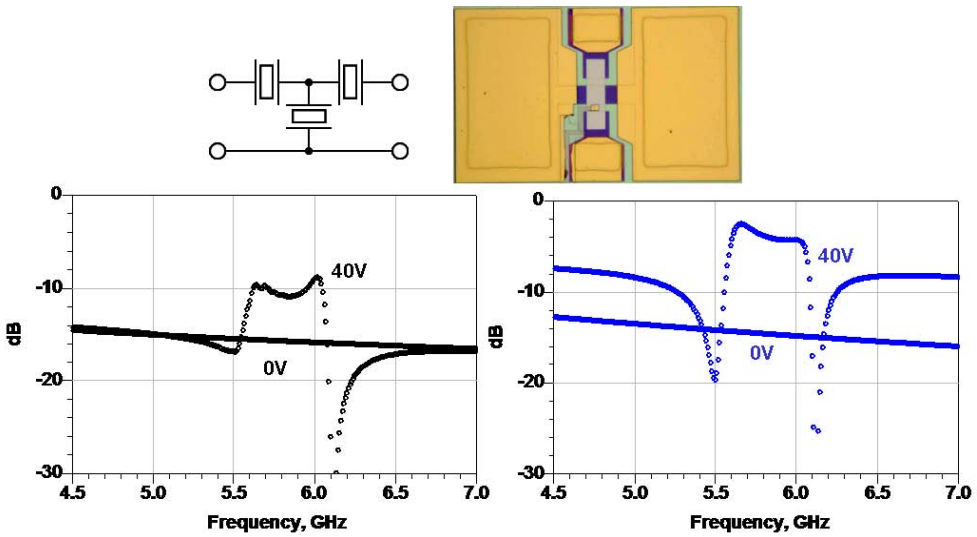

Figure 15 – Simple tee-filter using equal-sized series and shunt resonators. (a) raw data at 0V and 40V; (b) Modelled data with parasitics reduced.

Because of the close parallel with conventional SMR and FBAR technology, much is already known about circuit designs using BAW devices [14-16,18,31-32]. A standard approach for single-ended (unbalanced) circuits is a simple "ladder" network. The tee-filter shown in Figure 15 is essentially the simplest possible ladder filter, although it is important to recognize that even our first results could be significantly improved just through some minor adjustments to the electrode areas and film thicknesses, irrespective of any further refinements in the underlying technology. Figure 16a illustrates how the performance could be improved by merely changing the relative capacitor sizes and resonant frequencies. Figure 16b then projects this result to a 5-element ladder.

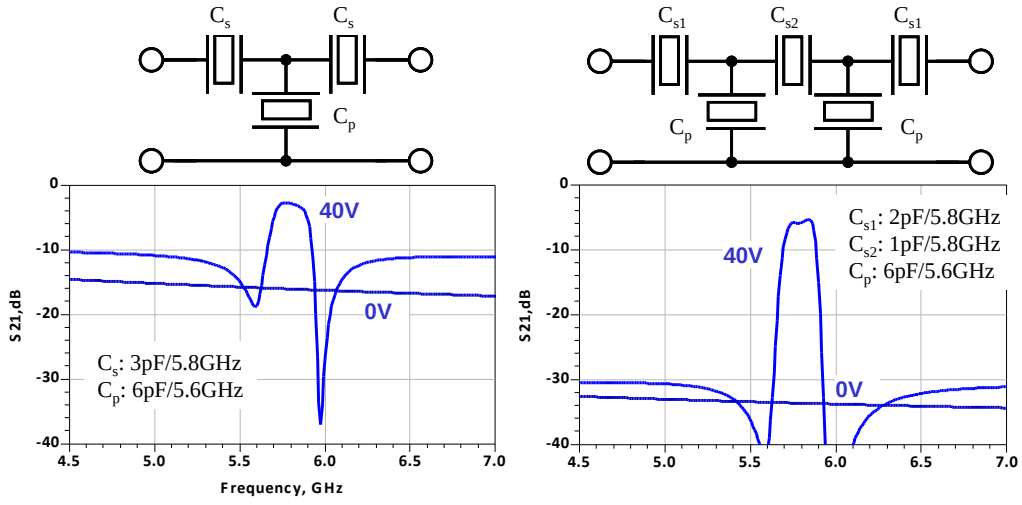

(a) (b)

Figure 16 –(a) Performance that would be obtained by adjusting the device capacitance and resonant frequency (thickness) in the tee-filter of Figure 15b, assuming no further improvements in device Q (Q=100) aside from the reduction in parasitics. (b) Projected improvement in moving to a 5-element ladder network.

Bibliography

[1] S. Roberts, “Dielectric and piezoelectric properties of barium titanate” Phys. Rev., vol. 71, pp. 890-895 June 1947.

[2] W.P. Mason, “Electrostrictive effect in barium titanate Ceramics”, Phys. Rev., vol. 74, pp. 1134-1147, Nov 1948

[3] K. Morito, Y. Iwazaki, T. Suzuki, and M. Fujimoto, “Electric field induced piezoelectric resonance in the micrometer to millimeter waveband in a thin film SrTiO3 capacitor”, *J. Applied Phys.*, vol. 94, pp. 5199-5205, Oct 2003

[4] S. Tappe, U. Böttger, and R. Waser, “Electrostrictive resonances in Ba0.7Sr0.3TiO3 thin films at microwave frequencies”, *Applied Physics Lett.*, vol. 85, pp. 624-626, 26 July 2005

[5] G.N. Saddik, D.S. Boesch, S. Stemmer, R.A. York, “Strontium titanate DC electric field switchable and tunable bulk acoustic wave solidly mounted resonator”, IEEE International Microwave Symposium IMS2008, Atlanta, GA June 2008, pp. 1263-1266.

[6] G.N. Saddik, J. Son, S. Stemmer, and R. A. York, "Improvement of BST Solidly Mounted Resonator Quality Factor by Reduction in Electrode Surface Roughness" ISIF 2009 Conference, Sep. 2009.

[7] G. N. Saddik, D. S. Boesch, S. Stemmer, and R. A. York , “DC electric field tunable bulk acoustic wave solidly mounted resonator using SrTiO3”, Appl. Phys. Lett. 91 043501 (July 23 2007).

[8] Xinen Zhu; Phillips, J.D.; Mortazawi, A.; , "A DC Voltage Dependant Switchable Thin Film Bulk Wave Acoustic Resonator Using Ferroelectric Thin Film," Microwave Symposium Digest, 2007. IEEE/MTT-S International , vol., no., pp.671-674, 3-8 June 2007

[9] Xinen Zhu; Lee, V.; Phillips, J.; Mortazawi, A.; , "An Intrinsically Switchable FBAR Filter Based on Barium Titanate Thin Films," Microwave and Wireless Components Letters, IEEE , vol.19, no.6, pp.359-361, June 2009

[10] J. Berge, A. Vorobiev, W. Steichen, and S. Gevorgian, “Tunable Solidly Mounted Thin Film Bulk Acoustic Resonators Based on $Ba_xSr_{1-x}TiO_3$ Films”, IEEE Microwave Wireless Comp. Lett., vol 17, pp. 655-657, 2007

[11] J. Berge, M.Norling, A.Vorobiev, S.Gevorgian, “Field and temperature dependent parameters of the dc field induced resonances in BaxSr1−xTiO3-based tunable thin film bulk acoustic resonators”, J. Applied Physics, 103, 064508, 2008

[12] A. Noeth, T. Yamada, V. O. Sherman, P. Muralt, A. K. Tagantsev, and N. Setter, “Tuning of direct current bias-induced resonances in micromachined $Ba_{0.3}Sr_{0.7}TiO_3$ thin-film capacitors”, Journal Of Applied Physics 102, 114110, 2007

[13] A. Volatier,E. Defaÿ, M. Aïd, A. N’hari, P. Ancey, B. Dubus, “Switchable and tunable strontium titanate electrostrictive bulk acoustic wave resonator integrated with a Bragg mirror”, Applied Physics Letters 92, 032906 2008.

[14] K.M.Lakin, “A review of thin-film resonator technology,” IEEE Microwave Magazine, pp.61-67, Dec 2003.

[15] F. Z. Bi and B.P. Barber, “Bulk Acoustic Wave RF Technology”, IEEE Microwave Magazine, pp. 65-80, Oct 2008

[16] R. Aigner, “SAW and BAW Technologies for RF Filter Applications: A Review of the Relative Strengths and Weaknesses”, 2008 *IEEE International Ultrasonics Symposium Proceedings*, pp. 582-589

[17] J.F. Rosenbaum, *Bulk Acoustic Wave Theory and Devices*, Artech House: Boston, 1988

[18] Y. Satoh, T. Nishihara, T. Yokoyama, M. Ueda And T. Miyashita, “Development of Piezoelectric Thin Film Resonator and Its Impact on Future Wireless Communication Systems”, *Japanese Journal of Applied Physics* Vol. 44, No. 5A, 2005, pp. 2883–2894

[19] R. Krimholtz, D.A. Leedhom, and G.L. Matthaei, “New equivalent circuit for elementary piezoelectric transducers”, *IEE Electron Lett.*, vol. 6, pp. 398-399, 1970

[20] A. A. Shirakawa, K.-M. Pham, P. Jarry, E. Kerhervé, “Design of FBAR Filters at High Frequency Bands,” Int. J. of RF and Microw. CAE, vol. 17, pp. 115-122, 2007.

[21] J.-H. Kim, S-H. Lee, J-H Ahn, and J-K Lee, “AlN piezoelectric materials for wireless communication thin film components,” J. of Ceramic Process. Res., vol. 3, no. 1, pp. 25-28 (2002).

[22] C.-J. Chung, Y.-C. Chen, C.-C. Cheng, C.-L. Wei, and K.-S. Kao, “Influence of Surface Roughness of Bragg Reflectors on Resonance Characteristics of Solidly-Mounted Resonators,” IEEE Trans. On Ultras. Ferroe. And Freq. control, vol. 54, no. 4, April 2007.

[23] S. Marksteiner, J. Kaitila, G. G. Fattinger and R. Aigner, “Optimization of Acoustic Mirrors for Solidly Mounted BAW Resonators”, 2005 IEEE Ultrasonics Symposium, pp. 329-332

[24] R. Aigner , “Bringing BAW Technology into Volume Production: The Ten Commandments and the Seven Deadly Sins”, IEEE Int. Symp. Acoust. Wave. Dev. for Future Mobile Communication Syst, 2007

[25] J. Enlund, D. Martin, V. Yantchev, I. Katardjiev, “Solidly mounted thin film electro-acoustic resonator utilizing a conductive Bragg reflector”, Sensors and Actuators A 141 (2008) 598–602

[26] J. Enlund*, I. Katardjiev and D. M. Martin, “Fabrication and Evaluation of an "Electrodeless" Solidly Mounted Thin Film Electroacoustic Resonator”, 2005 IEEE Ultrasonics Symposium, pp. 1837-1839

[27] C-L Wei, Y-C chen, C-C Cheng, K-S Kao, “Solidly mounted resonators consisting of a molybdenum and titanium Bragg reflector”, Appl. Phys. A 90, 501–506 (2008)

[28] R. Thalhammer and R. Aigner, “Energy loss mechanisms in SMR–type BAW devices”, IEEE *International Microwave Symposium*, pp. 226-228, IMS 2005

[29] G. G. Fattinger, S. Marksteiner, J. Kaitila, and R. Aigner, “Optimization of Acoustic Dispersion for High Performance Thin Film BAW Resonators”, 2005 IEEE Ultrasonics Symposium, pp. 1175-1178

[30] K.M. Lakin, G.R. Kline, and K.T. McCarron, “Thin Film Bulk Acoustic Wave Filters for GPS” IEEE Ultrasonics Symposium pp. 471-476 1992.

[31] K.M. Lakin, “Modeling of Thin Film Resonators and Filters” IEEE MTT-S Digest, pp. 149-152, 1992.

[32] K.M. Lakin, G.R. Kline, K.T. McCarron, “High-Q Microwave Acoustic Resonators and Filters” IEEE Trans. Microwave Theory Tech., Vol. 41, No. 12, p. 2139-2146, Dec. 1993.

[33] K. P. Lee, K. B. Jung, A.Srivastava, D. Kumar, R. K. Singh and S. J. Pearton, “High Density Dry Etching Of (Ba,Sr)TiO3 And LaNiO3”, Mat. Res. Soc. Symp. Proc. Vol. 596, pp. 91-96, 2000

[34] B. Jalan, R. Engel-Herbert, N. J. Wright, and S. Stemmer, Growth of high-quality SrTiO3 films using a hybrid molecular beam epitaxy approach, J. Vac. Sci. Technol. A 27, 461-464 (2009). http://link.aip.org/link/?JVA/27/461/1

[35] B. Jalan, P. Moetakef, and S. Stemmer, Molecular beam epitaxy of SrTiO3 with a growth window, Appl. Phys. Lett. 95, 032906 (2009). http://link.aip.org/link/?APPLAB/95/032906/1